DSPACE

https://dspace.org/

Ab initio study of p and ntype doping of twodimensional MoO2 investigation of a pnhomojunction

Kevin Ndang Amassa; Anne Justine Etindele; Dick Hartmann Douma; Stephane Kenmoe; Nithayanathan Chetty

https://hdl.handle.net/10539/41467
SCOPUS

Downloaded from a DSpace repository. https://dspace.org/

Journal of Physics Communications

PAPER

Ab initio study of p- and n-type doping of two-dimensional MoO_2: investigation of a pn-homojunction

Kevin Ndang Amassa[1], **Anne Justine Etindele**[2,*], **Dick Hartmann Douma**[3], **Stephane Kenmoe**[4,*] and **Chetty Nithaya**[5]

[1] University of Yaounde I, Department of Physics, Yaounde, Cameroon
[2] Ecole Normale Superieure, University of Yaounde I, Yaounde, Cameroon
[3] Groupe de Simulations Numériques en Magnétisme et Catalyse, Faculté des Sciences et Techniques, Université Marien Ngouabi, Brazzaville B.P. 69, Congo
[4] Department of Chemistry, University of Duisburg-Essen, Universitätsstr. 2, 45141 Essen, Germany
[5] University of the Witwatersrand, Faculty of Science, Johannesburg, South Africa
* Authors to whom any correspondence should be addressed.

E-mail: anne.etindele@univ-yaounde1.cm **and** stephane.kenmoe@uni-due.de

Keywords: MoO_2, p- and n-type doping, stacking, charge transfer, p-n jonction

OPEN ACCESS

RECEIVED
15 January 2024

REVISED
6 February 2024

ACCEPTED FOR PUBLICATION
16 February 2024

PUBLISHED
29 February 2024

Original content from this work may be used under the terms of the Creative Commons Attribution 4.0 licence.

Any further distribution of this work must maintain attribution to the author(s) and the title of the work, journal citation and DOI.

Abstract

Based on density functional theory, we studied the effect of p- and n-type doping on the structural and electronic properties of MoO_2 monolayers and bilayers. We used niobium (Nb) and nitrogen (N) as p-type dopants, and technetium (Tc) and fluorine (F) as n-type dopants through atomic substitutions. Our study shows that the presence of a substituent in the 4×4 supercell of MoO_2 leads to a slight distortion and negligible modification of the lattice parameter. Both p- and n-type doped monolayers exhibit a metallic character. The bilayers obtained by vertically stacking n-p doped monolayers all exhibit a metallic character, as their band diagrams do not show a band gap. The study of their charge difference highlights a physisorption phenomenon. This type of material, which features a nucleophilic site in the p-doped region and an electrophilic site in the n-doped region, is a promising candidate for catalysis. When n-type and p-type doped monolayers are horizontally joined, the resulting stack exhibits a semi-conductor behavior.The special feature of this stacking is that we obtain a true pn junction, that is a space charge zone associated with a potential jump. For its application in infrared junction diodes, we have demonstrated both quantitatively and qualitatively the existence of a potential jump at the junction.

1. Introduction

Transition metal dichalcogenide (TMDC) and dioxide (TMDO) monolayers with chemical formula MX_2 (M, transition metal and X chalcogenide) have been the focus of considerable research due to their intriguing electronic, optical and mechanical properties [1–3]. Due to their distinct properties, they have application in energy storage systems (supercapacitors, Li-ion batteries) [4, 5], gas sensors [6], catalysis [7], field-effect transistors [8], optoelectronic/photonic devices [9], logic circuits [10] and memory devices [11]. The presence of defects in their structures has further expanded the range of potential applications. Among these defects, we have vacancies, substitutions, or atoms in interstitial sites. Point defects such as sulfur or molybdenum atom vacancies can create localized energy levels in the band gap, which alters the electronic transport properties [12, 13]. Doping plays a crucial role in many materials used in various technological applications [14, 15]. After the structural, electronic, optical, magnetic, and mechanical characterization of TMDCs [16–18], a significant portion of research is increasingly focused on the question of their doping, thus expanding the range of their applications. Doping is a process by which impurities are intentionally added to a material to modify its properties. In the case of TMDCs, it has been demonstrated that doping by substitution of metallic atoms or chalcogens allows for the modification of electronic and optical properties [19, 20], control of conductivity and

© 2024 The Author(s). Published by IOP Publishing Ltd

magnetization [21], improvement of catalytic properties [22], etc. The p-type (n-type) doping is the introduction of acceptor (donor) impurities. Baoshan Tang *et al* have developed a substitution doping method to convert single-layer and multi-layer WS2 into p-type from n-type by doping it with nitrogen, aiming at the fabrication of a field-effect transistor [23]. The first-principles study of the doping effects on the electronic and optical properties of Molybdenumdisulfide was conducted by Hua Zhang *et al* [24]. They performed doping of the p-type, n-type, and compensatory doping. However, both transistors and junction diodes are obtained by contacting a p-type doped semiconductor with an n-type doped semiconductor [25]. The contact between these two materials creates a diffusion movement, meaning that electrons from the N region fill the holes in the P region [26], creating a region without mobile carriers (called the depletion zone or space charge region), which results in the appearance of a potential difference and thus an internal electric field E that prevents the diffusion of electrons from the N region to the P region [27]. One can also observe a potential jump at the junction.

MoO_2 with the space group $P6_3/mmc$ has been proven to be a better candidate than other TMDCs for lithium [28], sodium, potassium, and calcium [29] battery anodes.

This paper aims to evaluate its potential as a base material for the fabrication of a pn junction. Firstly, we will describe the modifications in its structural and electronic properties when doped p-type and n-type. Secondly, we will assess its ability to form a space charge region when stacking two p-doped and n-doped monolayers. Finally, we will evaluate the potential barrier at the junction.

The organization of this manuscript is as follows: The method used and the computational details are presented in section 2. The results obtained on the structural and electronic properties of doped monolayers and bilayers are presented in section 3. Potential applications, including the pn junction, are presented in section 4. Finally, the main conclusions of this study are presented in section 5.

2. Computational details

The present calculations were performed within the framework of density functional theory (DFT) using the quantum espresso code package in the pseudopotential method with a plane wave basis. The generalized gradient approximation (GGA) was used in our calculations, taking into account the Van der Waals interactions between layers by introducing the DFT-D3 Grimme correction [30, 31]. The cutoff kinetic energy and Brillouin zone mesh were determined by a thorough convergence test. The Brillouin zone was sampled (Monkhorst–Packmethod) with $6 \times 6 \times 1$ K points, and a plane wave basis set with a cutoff kinetic energy of 680 eV was used. The atomic coordinates, size, and shape of the primitive cell were treated by the Boydens-Fletcher-Goldfarb-Shanno (BFGS) algorithm. Relaxation calculations were stopped when the values of atomic forces were below $10^{-3} eV/\mathring{A}$. The self-consistent calculations were converged with an accuracy of $10^{-8} eV$. For p-type doping, we either replace in the supercell Mo with Nb or O wit N ; for n-type doping, we either replace in the supercell Mo with Tc or O with F. In such a way that the form structure can be note as $Mo_{1-x}Nb_xO_2$, $MoO_{2-y}N_y$ $Mo_{1-x}Tc_xO_2$ and $MoO_{2-y}F_y$ respectively. We have used the surrounding atoms so as to diminish the distorsions caused by these dopants in the supercell. The percentage of dopant atoms x or y is equal to 2.083% for the 4×4 cell. The reason for selecting a 4×4 supercell of molybdenum dioxide is because it allows for a realistic doping rate of 2.083% by substituting one oxygen atom with a dopant atom, while also minimizing interactions between dopant atoms. Additionally, a preliminary test examining the energy per atom as the supercell size increases indicates a noticeable variation starting from this size. Thermodynamic stability is verified by calculating the formation enthalpy given by the relationship (1) [23]:

$$E_f = E(MoO_2A) - m \times E(Mo) - n \times E(O) - E(d), \tag{1}$$

where $E(MoO_2A)$, $E(Mo)$, $E(O)$, $E(d)$, m, and n are respectively the energy of the doped monolayer, the energy of molybdenum, the energy of oxygen, the energy of the dopant, the number of molybdenum atoms, and the number of oxygen atoms. Two types of stacking of pristine and doped supercell are studied: a vertical stacking and a horizontal stacking. The potential jump at the junction is investigated using the bulk plus band lineup method. In this method, the conduction band offset and the valence band offset are calculated. The valence band oset (Φ_{VBO}) and the conduction band oset (Φ_{CBO}) can be expressed as the following equations [32]:

$$\begin{aligned} \Phi_{VBO}^{A-B} &= \mu_A - \mu_B + e\Delta_{ISR} \\ \Phi_{CBO}^{A-B} &= \mu_A - \mu_B + e\Delta_{ISR} + E_g^A - E_g^B \end{aligned} \tag{2}$$

In the equations provided above, the symbol μ represents the difference in energy between the highest point of the valence band (VBM) and the average electrostatic potential in the bulk environment. The superscript and subscript A/B indicate the semiconductor A/B. E_g the band gap energy. Meanwhile, $e\Delta_{ISR}$ refers to the difference in average electrostatic potential energies across the interface.

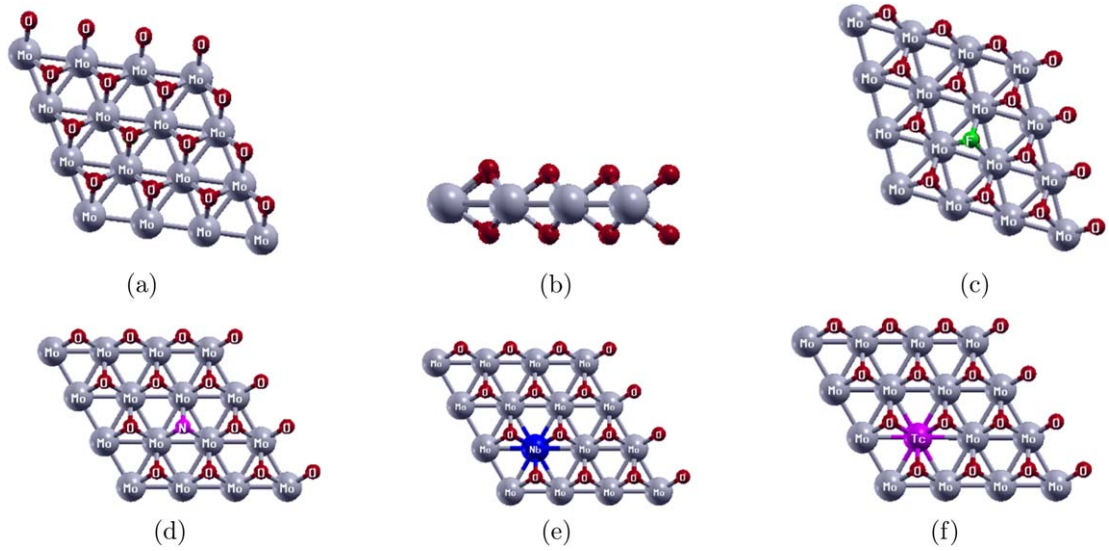


Figure 1. *Undoped MoO_2 cells.* (a) and (b) Top and side views of a non-doped 4 × 4 cell, (c), (d), (e), and (f) cells doped with Fluorine, Nitrogen, Niobium, and Technetium, respectively.

3. Results and discussion

3.1. p- and n-type doped MoO_2 monolayer

3.1.1. Structural Properties

The pristine and doped structures are shown in figure 1, where Mo and O atoms alternate at the vertices of the hexagon. In these structures, an atomic plane of Mo is sandwiched between two atomic planes of O to form hexagonal covalent bonds. The structural optimization parameters obtained for the pristine monolayer using the PBE method gave Mo-Mo distances of 2.825 $\mathring{A}$, Mo-O distances of 2.037 $\mathring{A}$, and O-O distances of 2.44 $\mathring{A}$. These results are consistent with those reported in the literature [16, 33, 34]. For the undoped monolayer, these results are in agreement with those reported in the literature. The structural parameters obtained for the doped monolayers are summarized in the table 1(a).

When comparing the results obtained with those of the pristine structure, we notice a slight distortion of the supercells in the presence of dopants. The lattice parameter of 2.83 angstroms in the presence of dopants is practically equal to that of the pristine MoO_2, due to the low kinetics of the dopants. The supercells have not been significantly modified and will be used for the rest of our calculations. The dopants Nb and Tc are similar in size compared with Mo, and N and F similar in size to O and so we don't expect any changes to the symmetry.

Thermodynamic stability was studied by calculating the energy or enthalpy of formation of the molecule. The results obtained for each structure are summarized in table 1. All these values are negative, indicating an exothermic formation process.

3.1.2. Electronic properties

The band structure of the 4 × 4 supercell of MoO_2 is shown in figure 2(a). This structure shows that MoO_2 is an indirect gap semiconductor with a gap value of approximately 0.97eV, this value is agreement with Ataca *et al* [16]. The valence band maximum (VBM) is located at the Γ point and the conduction band minimum (CBM) at the K point. The analysis of the projected density of states figure 2(b) shows that states near the Fermi level are a combination of Mo 4d orbitals and O 2p orbitals. These results are consistent with those found in the literature [35].

The study of the effect of dopants shows that doping with Nb and N induce a lifting of the conduction band, a shift of the Fermi level towards the valence band, and a partial occupation of the highest valence band. In doping with Tc and F, we observe a lowering of the conduction band, a closer proximity of the Fermi level to the conduction band, and a partial occupation of the lowest conduction band. These observations show that we have indeed achieved P-type doping on one hand and N-type doping on the other hand, and that in the presence of dopants the material has acquired a metallic character, which is consistent with previous results [36, 37]. The band structures of the different cells are represented in figure 3.

The projected density of states of the different structures are given in figure 4. One can notice the appearance of new orbitals in the formation of chemical bonds. Indeed 2p orbitals is observed for doping with N and F, and

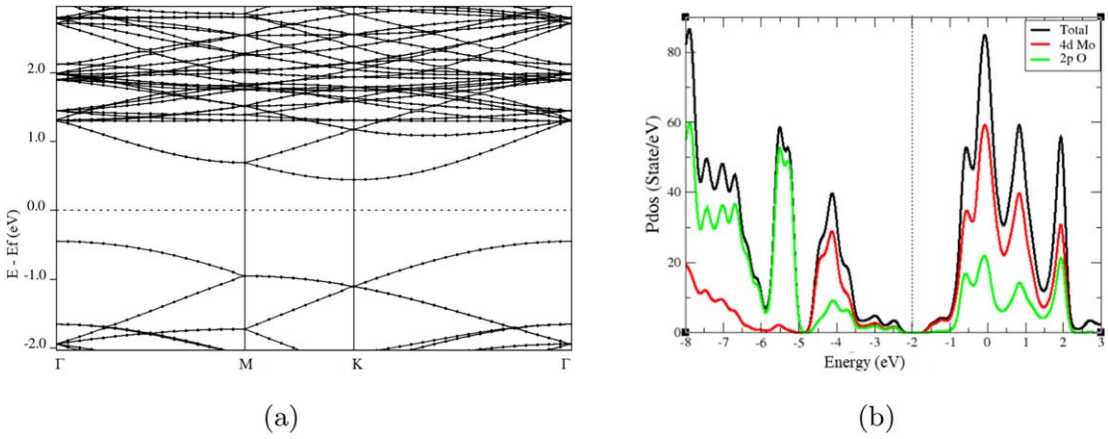


Figure 2. (a) Band structure of undoped MoO_2. (b) Projected density of states of MoO_2. The Fermi level is taken as a reference and represented by the dashed line.

Table 1. Interatomic distances and formation energy of doped structures.

(a) Interatomic distances in the different supercells.

	Bonds	Distances
Doping with N	Mo-Mo	2.8234
	Mo-N	2.0254
	O-N	2.4507
Doping with Nb	Mo-Nb	2.8378
	Nb-O	2.0423
	O-O	2.4501
Doping F	Mo-Mo	2.8342
	Mo-F	2.0435
	O-F	2.4376
Doping with Tc	Mo-Tc	2.8301
	Tc-O	2.0356
	O-O	2.4362

(b) Formation energy of doped structures.

Structures	Formation energy(Ry)
MoO_2-N	−0.695
MoO_2-Nb	−1.031
MoO_2-F	−0.361
MoO_2-Tc	−1.146

5d orbitals for doping with Tc and Nb. The presence of new peaks circled on figure 4 in the total density indicates the emergence of new acceptor states for P-type doping and donor states for N-type doping.

The charge difference was studied using the following mathematical relationship (3). [23] :

$$\Delta\rho = \rho_{d+MoO_2} - \rho_d - \rho_{MoO_2}, \tag{3}$$

where ρ_{d+MoO_2} is the charge density of MoO_2 plus impurity, ρ_d is the charge density of the impurity, and ρ_{MoO_2} is the charge density in the absence of impurity. The results obtained are summarized in figure 5. The analysis of these results shows, for doping with Fluorine and Nitrogen, a depletion of charges around the dopant, and an accumulation of charges around adjacent Molybdenum atoms. For doping with Technetium and Niobium, there is a strong accumulation of charges around the dopant and a depletion of charges around neighboring oxygen atoms. This depletion/accumulation of charges highlights the formation of covalent bonds between the dopant and its neighboring atoms, ensuring the long-term stability of the material similar to previous studies [23, 38].

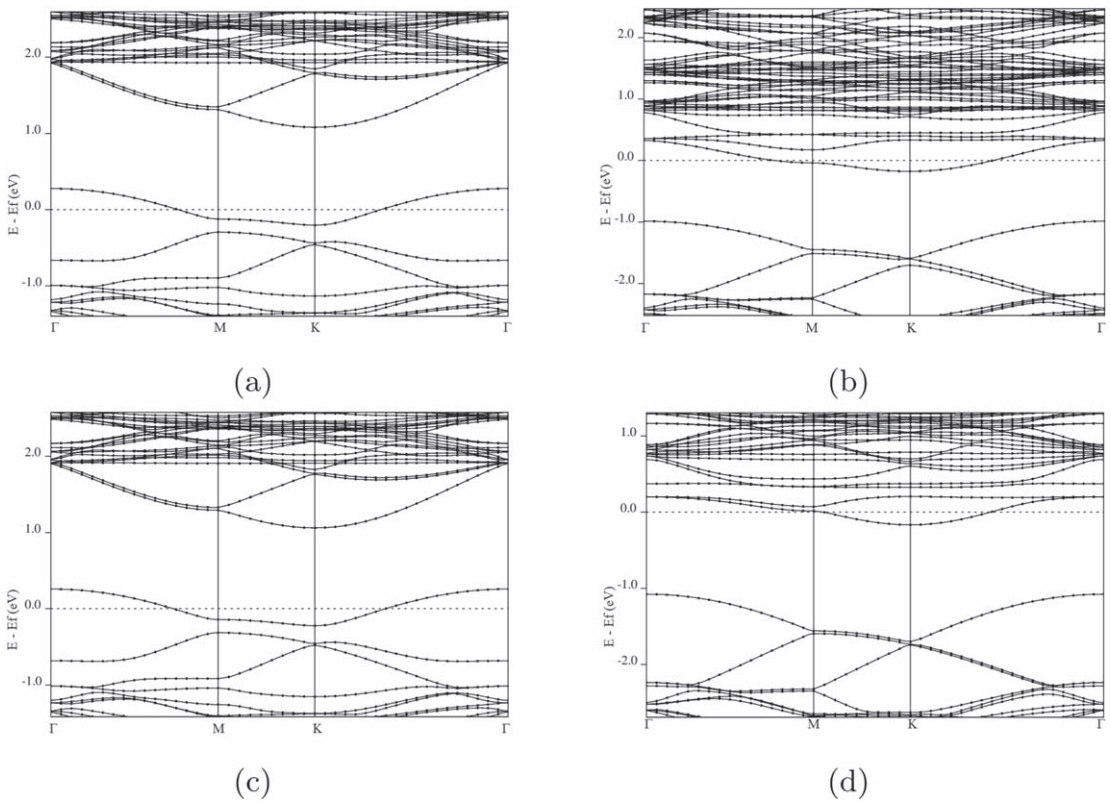


Figure 3. Band structure of MoO_2 for different types of dopants. (a) Doping with Niobium, (b) Doping with Technetium, (c) Doping with Nitrogen, (d) Doping with Fluorine. The Fermi energy is taken as a reference and is represented by the dashed line.

3.2. Pristine and doped MoO_2 stacking

3.2.1. Structural properties

A bilayer consists of the vertical stacking of two monolayers. There are several configurations on how the monolayers are stacked to form a bilayer [39]. Figure 6(a) shows the different stacking types for MoO_2. In our calculations, we will use the AA' stacking, which is the most stable structure [39]. Structural optimizations using the PBE method, taking into account Van-der-Waals corrections, show that the lattice parameter remains unchanged. Let c and d be the lattice parameter in z direction and the distance between two stacked layers. When d varies, for $c = 15\ \mathring{A}$, we observe two equilibrium points at $d = 5.93\ \mathring{A}$, and $d = 8.45\ \mathring{A}$. While we observe just one equilibrium point at $d = 5.93\ \mathring{A}$ as shown in figure 7. These results shown that to obtain an isolated bilayer, we can not start with a bulk, but it is necessary to stack two monolayers.

The calculation of the formation energy for $c = 15\ \mathring{A}$ yields $E_f = 2.053eV$, highlighting an endothermic formation process, while it gives $E = -1.37$ eV for $c = 22\ \mathring{A}$, highlighting an exothermic formation process.

Since in this second section, we will also study the possibility of fabricating a pn junction, we will study two types of 4×4 cell stackings (vertical and horizontal stacking), and doping will not be done randomly. In the vertical stacking, one layer will be doped P and the other N. The different doped structures are shown in figure 6. For the case of vertical stacking, we maintain the equilibrium distance obtained previously, which represents an approximation in this case, as the new equilibrium distance in the presence of dopants should be optimized. Relaxation calculations performed in the presence of dopants show a slight distortion of the cells due to the low kinetic energy of the dopants. The energy calculations for formation yield negative values, highlighting an exothermic formation process for all constructed structures.

3.2.2. Electronic properties

According to our calculations using the PBE method while taking into account van der Waals interactions between the sheets, both the vertical and lateral stackings are indirect gap semiconductors with gaps of approximately $0.86eV$ and $0.92eV$, respectively. In both cases, the valence band maximum (VBM) is localized at the Γ point and the conduction band minimum (CBM) at the K point. The band structures of undoped and doped vertical and horizontal stacks are presented in figure 8.

For vertical stackings, an absence of a band gap is observed. This result was predictable, as the monolayers forming the bilayer have a metallic character in the presence of dopants, and the lifting/lowering of the bands in

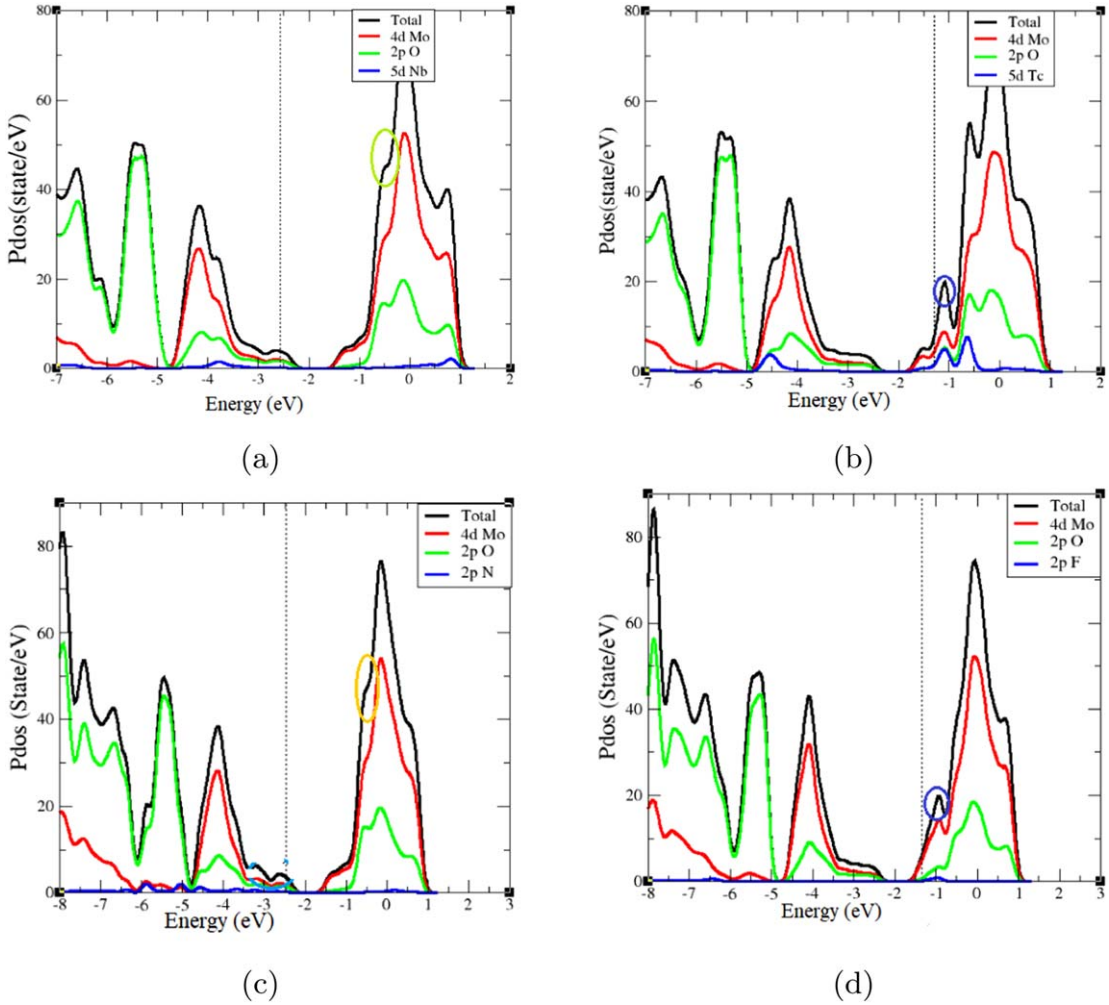


Figure 4. Projected density of states of MoO_2 for different types of dopants. (a) Doping with Niobium, (b) Doping with Technetium, (c) Doping with Nitrogen, (d) Doping with Fluorine. The Fermi energy is taken as a reference and is represented by the dashed line.

the P or N-doped cells cancelled out the gap in the bilayer formed by these two types of stackings. These analyses show that the P-N doped bilayer is conductive. In the case of horizontal stacking, a valence band, a conduction band, and a band gap are observed. The maximum of the valence band is located at the Γ point and the minimum of the conduction band at the K point. These observations show that horizontal stackings are semiconductors with gaps of approximately 0.683 and 0.79 eV respectively.

A study of charge difference was carried out. Analysis of the charge difference shows, in the case of vertical stacking, an accumulation of charge in the n-doped region and a depletion of charge in the p-doped region. This accumulation/depletion of charge is accentuated around the dopant. An arrangement of these charges is also observed on the internal surfaces between the two materials. These analyses highlight a physisorption phenomenon due to the presence of van der Waals interactions in the dipolar interactions between the two stacked sheets. Figure 9 presents these results. In the lateral stack, a strong charge accumulation zone is observed. This zone marks the separation between the two iron-doped cells, where there is a significant accumulation and depletion of charge. Negative charges are distributed in the P-doped zone, while positive charges are distributed in the n-doped zone. These analyses demonstrate a charge transfer and the creation of a pn junction, as well as a chemisorption phenomenon. These results are presented in figure 10.

4. Potential applications : a PN-junction

The horizontal stacks that we have manufactured can be used in PN junction diodes. To prove this, we perform a calculation to observe the electrostatic potential jump at the boundary between the two materials. The plane averaged electrostatic potential along the *y*-axis is computed according to the following equation:

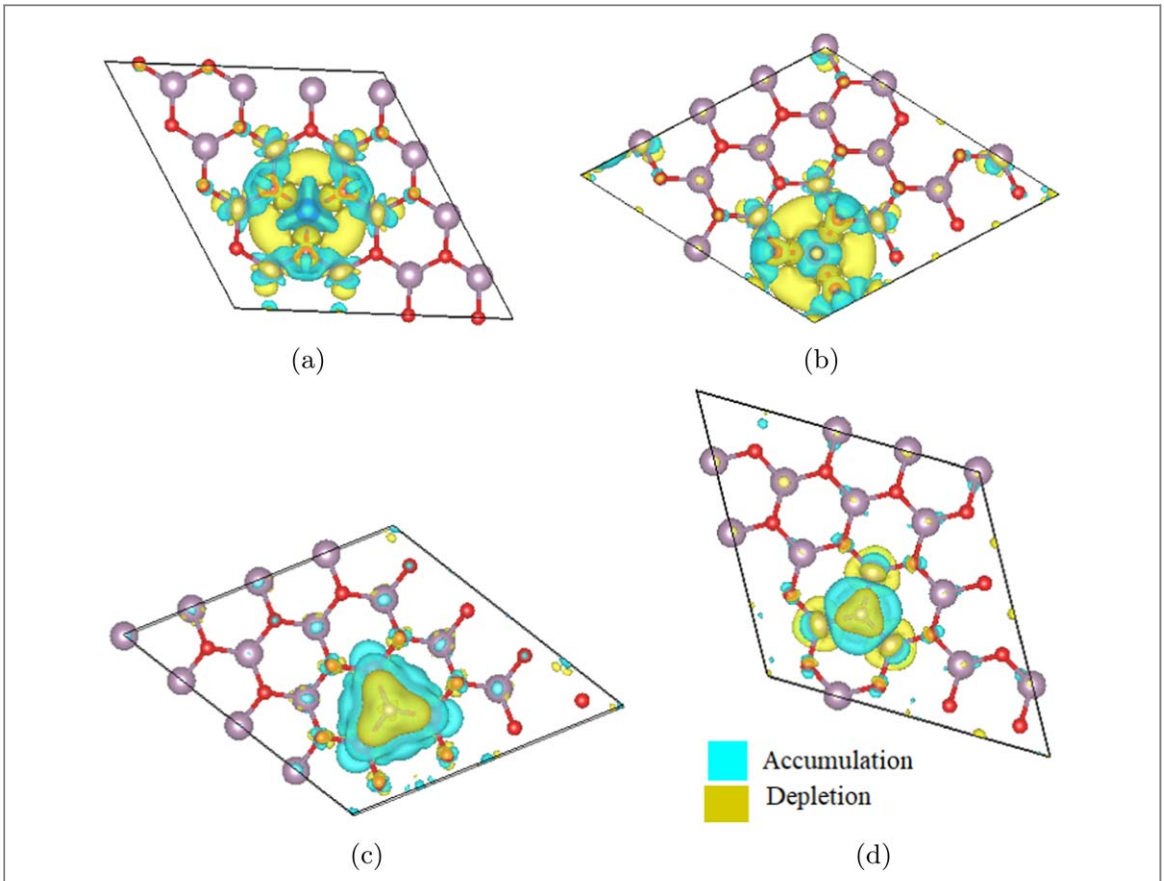


Figure 5. Charge difference of MoO_2 for different types of dopants. (a) Doping with Niobium, (b) Doping with Technetium, (c) Doping with Nitrogen, (d) Doping with Fluorine. The Fermi energy is taken as a reference and is represented by the dashed line. The precision of the isosurfaces has been set to $0.00286458e/\mathring{A}^2$.

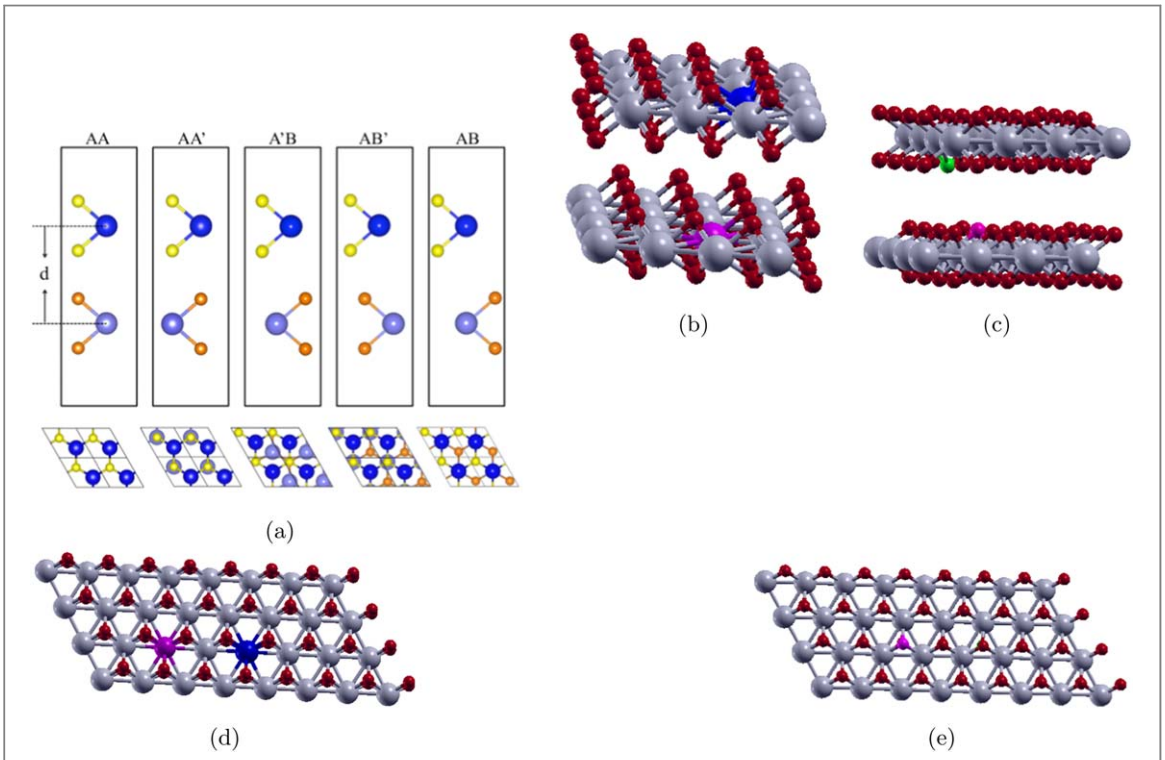


Figure 6. (a) Different possible vertical stackings [39]. (b), (c), (d), (e) Different dopant-doped 4×4 MoO_2 cell stackings used in this manuscript.

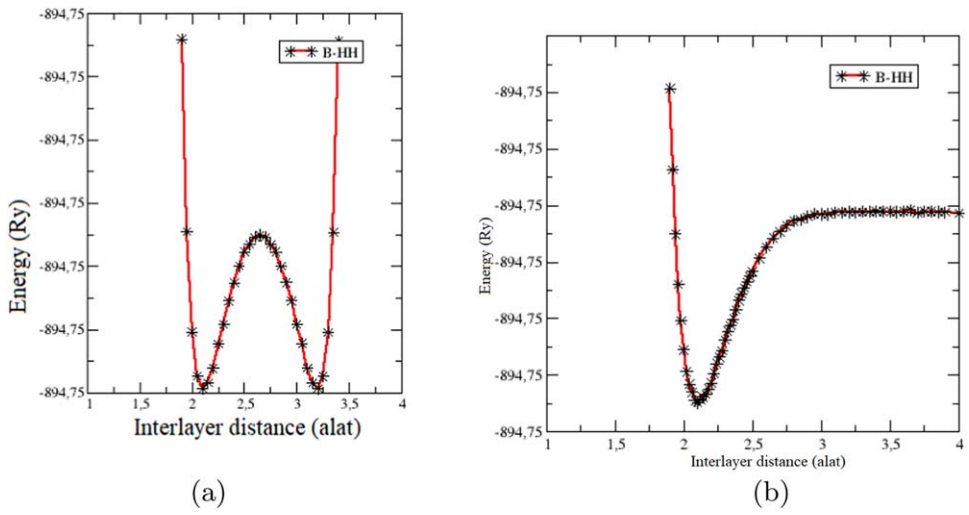


Figure 7. Variation of the total energy of the system as a function of the equilibrium distance between bilayers for $c = 15\ \mathring{A}$ (a) and $c = 22\ \mathring{A}$ (b).

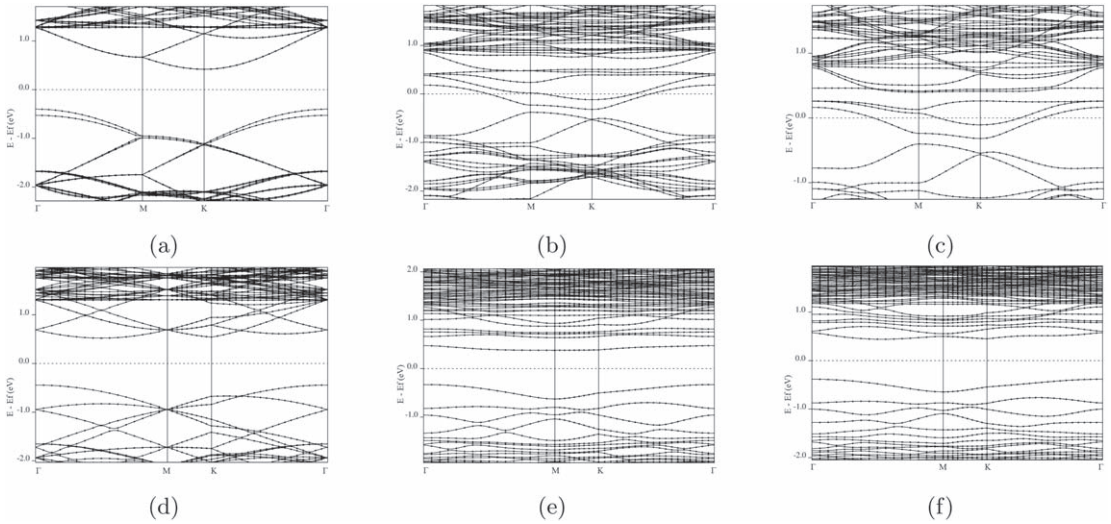


Figure 8. Band structure of undoped and doped 4×4 MoO_2 cell stackings. (a) Undoped vertical stacking, (b) Nb and Tc-doped vertical stacking, (c) N and F-doped vertical stacking, (d) Undoped horizontal stacking, (e) Nb and Tc-doped horizontal stacking, (f) N and F-doped horizontal stacking. The Fermi energy is taken as a reference and is represented by the dashed line.

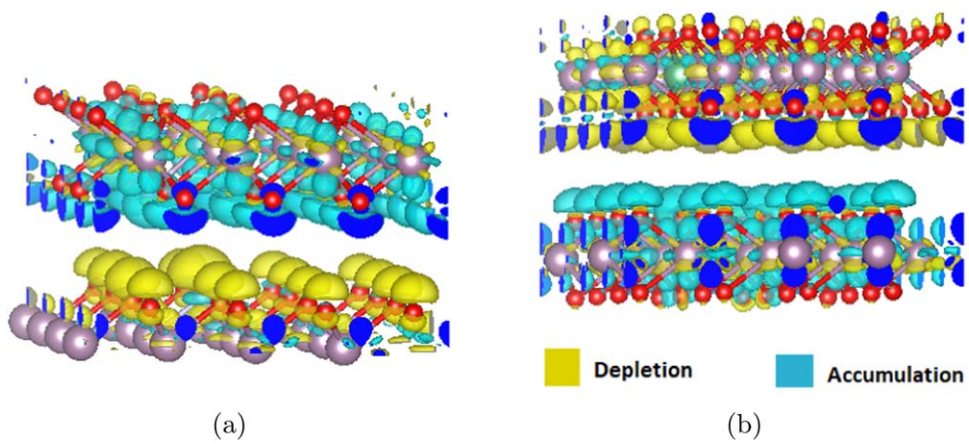


Figure 9. Difference in charges of vertical stacks of MoO_2. The precision of the isosurfaces was set to $0.00037e/\ \mathring{A}^3$. (a) The top surface is doped with F and the bottom surface is doped N. (b) The top surface is doped Nb and the bottom surface is doped Tc.

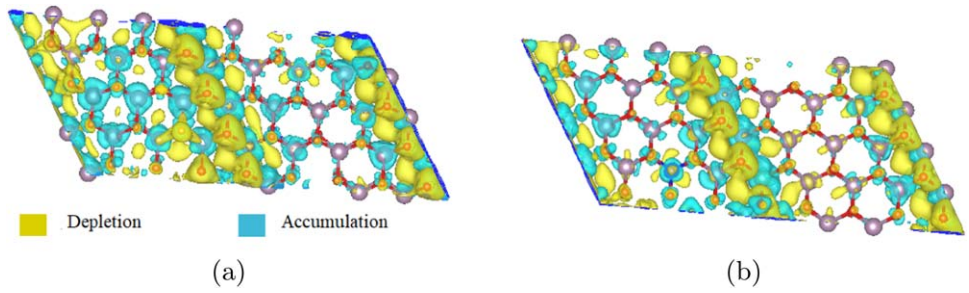


Figure 10. Difference in charges of horizontal stacks of MoO_2. The precision of the isosurfaces was set to $0.00037e/\mathring{A}^3$. (a) Doping with N(left) and F(right). (b) Doping with Tc(left) and Nb (right).

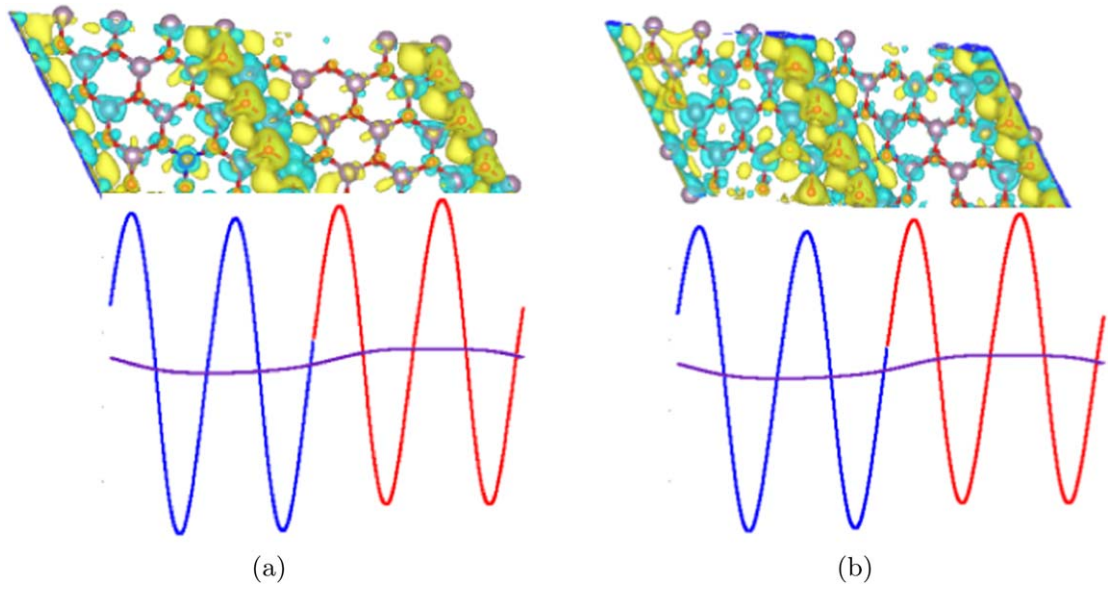


Figure 11. Average electrostatic potential variation along the y axis of the homo-junction. (a) Doping with Tc(left) and Nb(right). (b) Doping with N(left) and F(right). The blue and red lines represents the averaged potential in planes perpendicular to the y axis and the indigo line represents a smoothed average.

$$\overline{V}(y) = S^{-1}\int_S V(\vec{r})\,dxdz \tag{4}$$

S represents the area of the plane perpendicular to the y-direction, where x and z lie in that plane. V(r) is the electrostatic potential data generated by the PWSCF code. The results obtained are presented in figure 11. On these figures, we notice a harmonic variation of the potential, a jump of it at the boundary between the two materials. These results highlight the effective realization of a PN junction. The amplitudes of the oscillations are equal in both zones because it is the same material that has been doped. The indigo line represents the average of this potential. We obviously notice the potential jump at the junction between the two materials. This potential jump is equal to 0.04 eV for figure 11(a) and 0.03 eV for figure 11(b). However, each side of the material contains a single dopant and we notice an upward peak in the average potential on the right side and a downward peak in the average potential on the right material. This observation describes the periodicity of the pattern we used in our calculations. This result is in agreement with those in the literature.

5. Conclusion

In summary, our study has highlighted crucial properties in stacks of differently doped materials, revealing band gaps, physisorption and chemisorption phenomena. The physisorption phenomenon observed in the vertical stack would be useful in catalytic applications. The charge variation observed at the junction between the p- and n-type doped zones in the horizontal stack suggests promising applications in optoelectronics. In addition, for

specific applications such as infrared junction diodes, our quantitative and qualitative analysis has demonstrated the existence of a potential jump at the junction, underlining the potential at the junction useful for advanced electronic devices. These results pave the way for advances in the design of MoO_2-based semiconductor materials, offering interesting prospects for innovative electronic and catalytic applications.

Acknowledgments

The authors acknowledge the Centre for High Performance Computing (CHPC), South Africa, for providing computational resources to this research project. They are also thankful to Lodvert Tchibota Poaty, Serge Guy Nana Engo and Ousmanou Motapon for fruitful discussions. We acknowledge support by the Open Access Publication Fund of the University of Duisburg-Essen.

Data availability statement

The data that support the findings of this study are available upon reasonable request from the authors.

ORCID iDs

Stephane Kenmoe https://orcid.org/0000-0003-3622-2716

References

[1] Wang Q H, Kalantar-Zadeh K, Kis A, Coleman J N and Strano M S 2012 Electronics and optoelectronics of two-dimensional transition metal dichalcogenides *Nat. Nanotechnol.* **7** 699–712
[2] Jariwala D, Sangwan V K, Lauhon L J, Marks T J and Hersam M C 2014 Emerging device applications for semiconducting two-dimensional transition metal dichalcogenides *ACS Nano* **8** 1102–20
[3] Gupta A, Sakthivel T and Seal S 2015 Recent development in 2d materials beyond graphene *Prog. Mater Sci.* **73** 44–126
[4] Zhang X, Zhang Z and Zhou Z 2018 Mxene-based materials for electrochemical energy storage *Journal of Energy Chemistry* **27** 73–85
[5] Zhao Y, Zhang Y, Yang Z, Yan Y and Sun K 2013 Synthesis of MoS_2 and MoO_2 for their applications in h2 generation and lithium ion batteries: a review *Sci. Technol. Adv. Mater.* **14** 043501
[6] Late D J *et al* 2013 Sensing behavior of atomically thin-layered MoS_2 transistors *ACS Nano* **7** 4879–91
[7] Li Y, Wang H, Xie L, Liang Y, Hong G and Dai H 2011 MoS_2 nanoparticles grown on graphene: an advanced catalyst for the hydrogen evolution reaction JACS **133** 7296–9
[8] Chhowalla M, Shin H S, Eda G, Li L J, Loh K P and Zhang H 2013 The chemistry of two-dimensional layered transition metal dichalcogenide nanosheets *Nat. Chem.* **5** 263–75
[9] Xu K, Wang Z, Du X, Safdar M, Jiang C and He J 2013 Atomic-layer triangular wse2 sheets: synthesis and layer-dependent photoluminescence property *Nanotechnology* **24** 465705
[10] Radisavljevic B, Whitwick M B and Kis A 2011 Integrated circuits and logic operations based on single-layer MoS_2 *ACS Nano* **5** 9934–8
[11] Bertolazzi S, Krasnozhon D and Kis A 2013 Nonvolatile memory cells based on MoS_2/graphene heterostructures *ACS Nano* **7** 3246–52
[12] Gali S M, Pershin A, Lherbier A, Charlier J C and Beljonne D 2020 Electronic and transport properties in defective MoS_2: impact of sulfur vacancies *The Journal of Physical Chemistry* C **124** 15076–84
[13] Schmidt H, Giustiniano F and Eda G 2015 Electronic transport properties of transition metal dichalcogenide field-effect devices: surface and interface effects *Chem. Soc. Rev.* **44** 7715–36
[14] Bhargava R 1996 Doped nanocrystalline materialsphysics and applications *J. Lumin.* **70** 85–94
[15] Di Valentin C, Pacchioni G and Selloni A 2009 Reduced and n-type doped tio2: nature of ti3+ species *The Journal of Physical Chemistry* C **113** 20543–52
[16] Ataca C, Sahin H and Ciraci S 2012 Stable, single-layer mx2 transition-metal oxides and dichalcogenides in a honeycomb-like structure *The Journal of Physical Chemistry* C **116** 8983–99
[17] Mashmool A, Saeidi P, Yalameha S and Nourbakhsh Z 2020 First principles calculations of structural, electronic and optical properties MoX_2 (x=s, se) metal dichalcogenides and their nano-layers *J. Magn. Magn. Mater.* **503** 166572
[18] Tang W, Rassay S and Ravindra N 2017 Electronic & optical properties of transition-metal dichalcogenides *Madridge J Nano Tech* **2** 59–65
[19] Haldar D, Ghosh A, Bose S, Mondal S, Ghorai U K and Saha S K 2018 Defect induced photoluminescence in MoS_2 quantum dots and effect of eu3+/tb3+ co-doping towards efficient white light emission *Opt. Mater.* **79** 12–20
[20] Khan M J I, Liu J, Latif A, Majeed I, Ullah H, Asghar M and Ahmad J 2022 Investigating structural, electronic, magnetic, and optical properties of co-doped and co-x (x=fe, mn) co-doped MoS_2 for optoelectronic applications *J. Mol. Model.* **28** 310
[21] Khan M J I *et al* 2023 Exploring structural, electronic, magnetic, and optical properties of ceo2-x (x=pt/ni) doped and pt-ni co-doped ceo2 for optoelectronic applications *Phys. Scr.* **98** 045914
[22] Sathiyan K, Mondal T, Mukherjee P, Patra S G, Pitussi I, Kornweitz H, Bar-Ziv R and Zidki T 2022 Enhancing the catalytic oer performance of MoS_2 via fe and co doping *Nanoscale* **14** 16148–55
[23] Tang B *et al* 2018 Direct n-to p-type channel conversion in monolayer/few-layer ws2 field-effect transistors by atomic nitrogen treatment *ACS Nano* **12** 2506–13
[24] Zhang H, Zhou W, Yang Z, Wu S, Ouyang F and Xu H 2017 A first-principles study of impurity effects on monolayer mos2: bandgap dominated by donor impurities *Mater. Res. Express* **4** 126301

[25] Chuang H J, Tan X, Ghimire N J, Perera M M, Chamlagain B, Cheng M M C, Yan J, Mandrus D, Tomanek D and Zhou Z 2014 High mobility WSe_2 p-and n-type field-effect transistors contacted by highly doped graphene for low-resistance contacts *Nano Lett.* **14** 3594–601
[26] Shockley W 1949 The theory of p-n junctions in semiconductors and p-n junction transistors *Bell Syst. Tech. J.* **28** 435–89
[27] Harper C A 2004 *Electronic Materials and Processes Handbook* (McGraw-Hill Education)
[28] Zhou Y and Geng C 2017 A MoO_2 sheet as a promising electrode material: ultrafast li-diffusion and astonishing li-storage capacity *Nanotechnology* **28** 105402
[29] Rao Y C, Yu S, Gu X and Duan X M 2019 Prediction of MoO_2 as high capacity electrode material for (na, k, ca)-ion batteries *Appl. Surf. Sci.* **479** 64–9
[30] Grimme S, Antony J, Ehrlich S and Krieg H 2010 A consistent and accurate ab initio parametrization of density functional dispersion correction (dft-d) for the 94 elements h-pu *J. Chem. Phys.* **132** 154104
[31] Grimme S, Ehrlich S and Goerigk L 2011 Effect of the damping function in dispersion corrected density functional theory *J. Comput. Chem.* **32** 1456–65
[32] Tung R T and Kronik L 2018 Charge density and band offsets at heterovalent semiconductor interfaces *Adv. Theory Simul.* **1** 1700001
[33] Zeng F, Zhang W B and Tang B Y 2015 Electronic structures and elastic properties of monolayer and bilayer transition metal dichalcogenides MX_2 (m=mo, w; x=o, s, se, te): a comparative first-principles study *Chin. Phys.* B **24** 097103
[34] Yang L, Gao Q, Zhang Y, Tang Y and Wu Y 2008 Tremella-like molybdenum dioxide consisting of nanosheets as an anode material for lithium ion battery *Electrochem. Commun.* **10** 118–22
[35] Jian C, Cai Q, Hong W, Li J and Liu W 2018 Edge-riched $MoSe_2/MoO_2$ hybrid electrocatalyst for efficient hydrogen evolution reaction *Small* **14** 1703798
[36] Tian Y, Zhu Z, Ge Z, Sun A, Zhang Q, Huang S, Li H and Meng J 2020 Electronic and magnetic properties of 3d transition metal doped $MoSe_2$ monolayer *Physica E* **116** 113745
[37] Ouma C N, Obodo K O, Parlak C and Amolo G O 2020 Effect of 3d transition metal substitutional dopants and adatoms on monolayer TcS_2 ab initio insights *Physica E* **123** 114165
[38] Wang W, Wang X, Shan J, Yue L, Shao Z, Chen L, Lu D and Li Y 2023 Atomic-level design rules of metal-cation-doped catalysts: manipulating electron affinity/ionic radius of doped cations for accelerating sulfur redox kinetics in li-s batteries *Energy & Environmental Science* **16** 2669–83
[39] He J, Hummer K and Franchini C 2014 Stacking effects on the electronic and optical properties of bilayer transition metal dichalcogenides MoS_2, $MoSe_2$, WS_2, and WSe_2 *Phys. Rev.* B **89** 075409